Nanocompression of 20 nm Silver Nanoparticles: In situ Aberration-Corrected TEM and Atomistic Simulations

Christopher Earl Carlton, Fátima Zorro, Maria José Caturla, Toshihiro Aoki, Yimei Zhu, Jonathan Amodeo, Paulo Jorge Ferreira

C.E. Carlton, F. Zorro, M.J. Caturla, T. Aoki, Y. Zhu, J. Amodeo, P.J. Ferreira, Nanocompression of 20 nm Silver Nanoparticles: In situ Aberration-Corrected TEM and Atomistic Simulations, Small (2024) e2405292. https://doi.org/10.1002/smll.202405292

Nanocompression of 20 nm silver nanoparticles: *in-situ* aberration-corrected TEM and atomistic simulations

C.E. Carlton[1,2], F. Zorro[3,4], M.J. Caturla[5], T. Aoki[6], Y. Zhu[7], J. Amodeo[8], P.J. Ferreira[1,3,4*]

[1] Materials Science and Engineering Program, University of Texas at Austin, Austin, TX, 78712, USA

[2] Samsung Semiconductor, 12100 Samsung Blvd, Austin, TX 78754, USA

[3] INL - International Iberian Nanotechnology Laboratory, Av. Mestre José Veiga, 4715-330 Braga, Portugal

[4] Mechanical Engineering Department and IDMEC, Instituto Superior Técnico, University of Lisbon, Av. Rovisco Pais, 1049-001 Lisboa, Portugal

[5] Department of Applied Physics, University of Alicante, Carretera San Vicente del Raspeig, 03690 San Vicente del Raspeig, Alicante, Spain

[6]Irvine Materials Research Institute, 644 Engineering Tower, University of California at Irvine, Irvine, CA 92617, USA

[7] Department of Condensed Matter Physics and Materials Science, Brookhaven National Laboratory, Upton, NY 11973, USA

[8] Aix Marseille Université, Université de Toulon, CNRS, IM2NP, 13397 Marseille, France

*corresponding author

Keywords: Nanomechanics, Aberration-corrected TEM, Nanoparticles, Dislocations, Molecular Dynamics

Abstract: Single-crystalline nanoparticles play an increasingly important role in a wide variety of fields including pharmaceuticals, advanced materials, catalysts for fuel cells, energy materials, as well as environmental detection and monitoring. Yet, the deformation mechanisms of very small nanoparticles are still poorly understood, in particular the role played by single dislocations and

their interaction with surfaces. In this work, silver nanoparticles with particularly small dimensions (~20 nanometers in diameter) are compressed *in situ* in an aberration-corrected transmission electron microscopy and molecular dynamics simulations. During compression, the emergence of both dislocations and nanotwins were observed. However, these defects prove to be unstable and disappear upon removal of the indenter. Atomistic simulations confirm the role played by image stresses associated with the nearby surfaces and the reduction in dislocation line length as it approaches the free surface, thereby supporting the experimental observations. These results provide justification for the frequent observation of the absence of dislocations in nanoparticles of a few nanometers size during *in-situ* experiments, even after significant deformation. This phenomenon contributes to the self-healing of samples through dislocation ejection towards the surfaces.

Introduction

Nanoparticles (NPs) are subjected to intriguing size and shape effects due to their increased surface-to-volume ratio. While there are still many unanswered questions about NPs, reducing the characteristic length of crystals to the nanoscale has a significant impact on their mechanical properties. Among these properties, plastic deformation is critical for many applications, and thus, understanding the behavior of dislocations in NPs is essential to design and develop novel materials. For example, in pharmaceuticals, tablets are the desirable form of drug delivery, yet NPs need to be compacted to ensure easy administration to patients [1]. In the case of advanced materials, nanoparticles are typically embedded in composites to improve their mechanical properties [2]. In catalysis, it is well established that strain modifies the chemical properties of metallic systems [3,4]. For batteries, NPs forming the electrodes are commonly subjected to calendering, in conjunction with carbon and a binder, to increase the volumetric energy density and electrical conductivity [5]. Yet, most of the studies about the plastic deformation of nanoscale materials have focused on 1D (nanopillars, nanowires, nanorods, nanotubes), 2D (nanofilms), and 3D nanocrystalline (bulk) materials [6-14], as well as nanoscale metallic contacts [15-19].

The literature on the compression of individual NPs is sparser [20-23], particularly for sizes below 100 nm [24-29]. Wu et al. found a significant amount of nanotwins in Pb and Ge NPs [24], while Gerberich et al. [25,26] reported that Si nanospheres were superhard and exhibited reverse plastic

displacement. Mordehai et al. [27] performed nanomechanical testing of gold NPs ranging from 80 nm to 180 nm and reported a reduction in the strength of the particles for a decrease in particle size. They attributed these results to the ability of free surfaces to capture dislocations. However, no dislocation was observed due to the limitations of the technique used. To explain the absence of dislocations, Mordehai et al. [27] and Zhang et al. [28] performed molecular dynamics (MD) simulations and claimed that below a critical NP size, dislocations become unstable due to the presence of free surfaces. Kositski and Mordehai performed MD indentation simulations of α-Fe NPs and thin films, showing that, in contrast with recent observations in FCC metals, the indentation curves for the NPs and thin films were alike and that ½<111>{110} type dislocations were nucleated in six possible directions, but remained pinned to their nucleation sites [29].

Carlton and Ferreira [30] were the first to attempt to observe the behavior of dislocations in individual NPs with sizes < 100 nm using diffraction contrast *in-situ* transmission electron microscopy (TEM) nanocompression experiments. However, the delicate nature of these experiments, in particular tilting the NPs to proper diffraction conditions, makes these diffraction contrast *in-situ* TEM experiments very challenging. In some cases, the contrast of dislocations may actually result from various artifacts, such as strain contours and thickness fringes. To overcome these difficulties, Carlton and Ferreira [30] carried out phase contrast *in-situ* nanocompression TEM experiments. In this case, dislocations appeared during deformation, while upon removal of the indenter, the dislocations disappeared. Yet, the Burgers vector of the dislocations was difficult to establish and not determined; the atomic columns were not observed due to limitations in image resolution; the overlap of the indenter with the NP produced less interpretable images; and no computer simulations were performed to interpret the experimental results. These obstacles have not permitted the verification of the type of defects present during the deformation. Subsequently, J. Sun et al. [31] compressed sub-10 nm Ag NPs (partially bonded on the surface of a tungsten stip) onto ZrO_2 by *in situ* TEM. The authors claimed that the shape changes due to deformation were dominated by surface diffusion, with no sign of dislocation activity. However, the orientation of the particles with respect to the indenter was not determined nor the resolution was high enough to identify the atomic columns. Issa et al. have compressed MgO cubes with sizes < 100 nm, using diffraction contrast *in-situ* TEM [32, 33]. The authors observed the appearance of contrast bands,

upon compression, which suggested the presence of perfect dislocations, confirmed by the MD compression simulations [32], as well as surface dislocation nucleation and starvation events that result in the absence of dislocations, after unloading [33]. In another paper, Wagner et al. also reported the formation of dislocation embryos, leading to the onset of plasticity [34]. In addition, significant plastic deformation by partial dislocations was also observed [34]. Using high-pressure XRD, optical absorbance spectroscopy and MD simulations, Parakh et al. [35] have deformed 3.9 nm Au nanoparticles in the form of a thin film. They reported that the plastic deformation was governed by stacking faults through the nucleation of partial dislocations at the surface. Later, the same group [36] used post-compression TEM images to show that upon unloading the samples the amount of microtwins had decreased. More recently, Chen et al., showed that upon removing surface imperfections from MgO NPs, they observed a quasi-homogeneous surface nucleation of dislocations, leading to an increase of the compressive strength [37].

In the current paper, we perform, for the first time, aberration-corrected *in-situ* TEM nanocompression experiments in individual NPs with sizes < 20 nm, in combination with MD computer simulations. Under these conditions, we were able to resolve the atomic columns and orientation of the NPs, which in conjunction with MD simulations, allows us to identify unambiguously the type of defects operating during the nanocompression experiments, as well as monitor the behavior of the defects after the load is removed. In addition, it enabled us to determine the effect of the shape of both the Ag NPs and the indenter, as well as the orientation on the type of defect that nucleates at the surface of the NPs.

Deformation of silver nanoparticles using *in-situ* TEM nanocompression

Nearly spherical silver (Ag) NPs, provided by NovacentrixTM with a nominal size of 20 nm, were used for the *in-situ* TEM nanocompression experiments. Ag NPs are particularly suitable for these experiments as, in addition to exhibiting the classical FCC structure, they do not readily form a native oxide. The FCC structure is ideal as the types of defects caused by plastic deformation are for the most part well known, and the absence of an oxide layer is an important parameter of this study as it might greatly impact the overall mechanical properties at the nanoscale, where the thickness of an oxide layer may become a significant fraction of the overall sample dimensions.

Many nanocompression experiments were performed, yet to set the right orientation between the nanoindenter and the particle, such that the particle does not move upon indentation, and obtain the appropriate imaging conditions, it is very challenging. Thus, in this paper we have selected an experiment which allows us to make a complete dislocation analysis and simultaneously be representative of the behavior of this material.

In this context, phase contrast aberration-corrected TEM images were acquired before, during, and after nanocompression. To be able to locate the atomic positions in the phase contrast TEM images, a multislice computer simulation (using the simulaTEM software [38]) of the Ag NP was performed, based on the conditions used during the operation of the aberration-corrected JEOL 2200 TEM. As shown in the supplemental Figure S1, both the aberration-corrected phase contrast image (Figure S1-A) and the contrast transfer function (Figure S1-B) confirm that for a defocus of 14 Å and a spherical aberration coefficient of 1µm used in the experiments, the atomic columns exhibit a white contrast. A movie clip of the in-situ TEM nanocompression experiments can be seen in the supported file (Movie S1). In several other in-situ TEM experiments we performed, dislocations were also found, as shown for example in Figure S2, but the configuration discussed next (Figure 1) was found to be the best for a complete analysis. Although in this study we only present a limited number of particles due to the challenge of the in-situ TEM experiments at atomic scale (requires contact alignment, surface cleanliness, crystallographic orientation), our insightful observations of mechanical deformation behavior of nanoparticles open a door for future experiments.

Figure 1 shows an Ag NP with a size of approximately 20 nm (labelled I) before and during compression. We focused our analysis on the top region of NP I, as this area is not affected by the presence of a second NP (labelled II), which is in the background and is not contacted by the indenter during the entire *in-situ* TEM experiment. A detailed investigation of the NP I top region confirms that the sample is dislocation-free before compression, as shown by the continuous lattice planes (Figure 1B). After careful adjustment of focus, the W probe was brought into contact with the Ag NP. Figures 1C and D (the latter being digitally magnified) illustrate the time of contact between the indenter and NP I where the lattice fringes remain continuous. This confirms that the NP deforms only elastically at this stage, without any sign of dislocations. At this point we were

not able to identify whether the two particles I and II are connected through a neck or discontinued. However, Figures 1E-1G shows that particle II exhibits an in-plane anti-clock rotation of 48 degrees with respect to particle I.

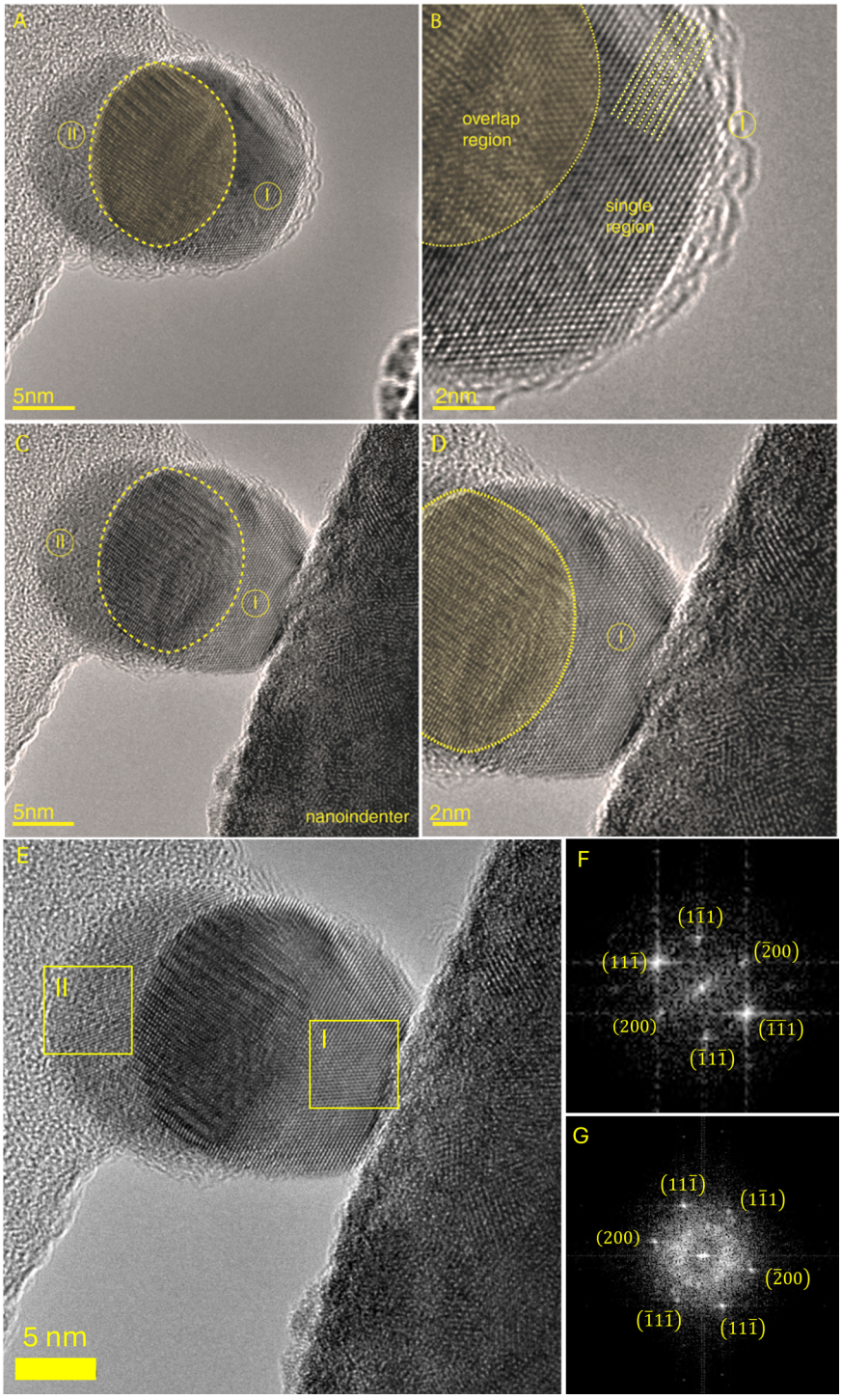

Fig. 1: Phase contrast TEM images taken from the *in-situ* nanoindentation experiment: A) The two NPs I and II before the experiment. The region highlighted in yellow represents where the overlap between the two NPs occurs. B) Magnification of the previous image displaying the NP I top region of interest. C) Initial contact between the NP and the indenter (time=2:30 in movie S1), D) Higher magnification of C). E) Overlap of particles I and II during nanoindentation. The yellow squares corresponding to particles I and II were used to acquire the FFTs shown in F) and G). F) FFT of particle I along the $[0\bar{1}\bar{1}]$ zone axis. G) FFT of particle II along the $[0\bar{1}\bar{1}]$ zone axis with an in-plane anti-clock rotation of 48 degrees with respect to I.

Dislocation nucleation and motion during *in-situ* TEM nanocompression

Figure 2 illustrates NP I under compression at a displacement of 3.6 nm. The inset in Figure 2A shows the FFT of the high-resolution image. The electron beam is oriented parallel to the $[0\bar{1}\bar{1}]$ direction. A careful examination of Figure 2A indicates a region within the NP where significant changes in contrast have occurred (region within the yellow box). This region was digitally magnified in Figure 2B, where a shear of two consecutive $(1\bar{1}\bar{1})$ planes is observed and attributed to a two-layer nanotwin, thus producing an extrinsic stacking-fault and a twin front. A detailed analysis of this defect shows that the twin front is bounded by two Shockley partial dislocations with Burgers vector b=$1/6[\bar{2}\bar{1}1]$, along two consecutive $[1\bar{1}1]$ planes, as shown in Figure 2C. The possible occurrence of a two-layer nanotwin in <111>-oriented Wulff-shaped Ag NPs under compression is confirmed by MD simulations (Figure 2D). At the end of the experiment, the indenter probe was moved back to examine the sample in a relaxed state, after deformation. Hereafter, the NP shows a defect-free atomic configuration, i.e. the two-layer nanotwin has left the sample after the indenter removal (inset images in Figure 2E).

The stress required to nucleate a dislocation (or a nanotwin) in NPs is usually larger than that required to activate glide. Thus, once defects are generated by the load imposed by the indenter, they are supposed to run across the NP and produce deformation. This mechanism is highlighted by the flat surface of the NP produced upon removing the indenter (Figure 2E), as this is possible only after significant plastic deformation. However, under certain conditions, dislocations and/or twins may remain stationary within the NP. This can happen if the stress imposed by the indenter

is compensated by other stress sources, in particular, i) image stresses induced by either the presence of nearby free surfaces or surfaces in contact with the indenter/substrate, ii) internal stresses caused by other dislocations inside the NP [39], and iii) gradient in shear stress as a function of depth due to the spherical/faceted shape of the particle. This is the case for the observed two-layer nanotwin, which remains stable while the indenter is in contact with the NP.

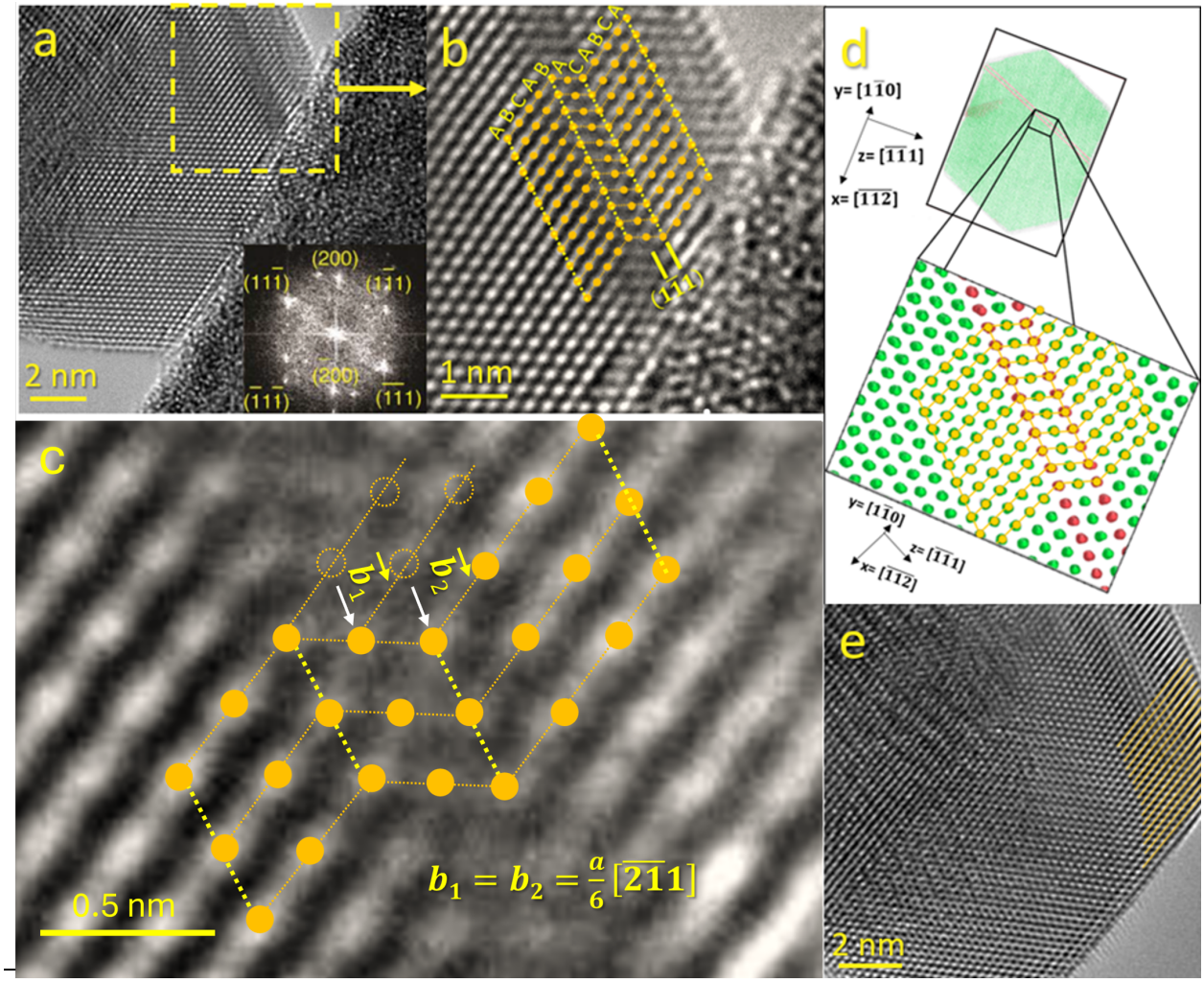

Fig. 2: Phase contrast TEM images of the nanoindentation experiment and MD simulation. A) NP being compressed, where changes in contrast can be found in the region within the yellow box (time=3:50 in movie S1). The FFT in the inset indicates that the electron beam is oriented parallel to the $[0\bar{1}1]$ direction. B) Magnification of region in image A showing the formation of a two-layer twin. C) Shear of two $a/6[\bar{2}\bar{1}1]$ Shockley partial dislocations along two consecutive $(1\bar{1}1)$ planes, which combine to form a two-layer nanotwin. D) MD simulation of a <111>-oriented Wulff-shaped Ag NP under compression. A two-layer twin is bounded by the atoms colored in red

(HCP local crystal structure). Atoms colored in green refer to the FCC's local crystalline structure. E) NP with a perfect registry of planes once the strain from the nanoindenter is released (time=12:50 in movie S1).

Additional MD simulations of Ag NP under compression were carried out in order to confirm these observations. The nanocompression method is based on the use of two virtual force fields, used as substrate and indenter [32, 40], and is illustrated in Figure 3A. Several indenter shapes and sample orientations were tested for spherical and Wulff-shaped NPs to reproduce the experimental conditions associated with <111>-oriented NPs. All the simulations were characterized by a two-stage deformation process, including an initial elastic deformation stage, followed by a plasticization of the NP induced by the nucleation of defects from the sample surfaces.

The orientation and the shape of the NPs play a key role in the type of defects that occur during the deformation process in the simulations. In particular, plastic deformation induced by the nucleation of 1/6<112>{111} Shockley partial dislocations is observed for <111>-oriented spherical particles compressed using a flat punch (Figure 3B), while <110>-oriented spheres (using a flat punch) and <111> oriented Wulff-shaped NPs (using a spherical indenter) exhibit the nucleation of both Shockley partials and ½<110> prismatic loops (Burger vector does not lie in the plane of the loop) made of {111} interconnected dislocations (Figures 3C-D). No nanotwins are noticed in these cases. While the nucleation of Shockley partial dislocations is quite common in FCC metal nanostructures [41-43], the occurrence of prismatic loops is more frequently observed in nanoindentation and irradiation cases [44-46]. In addition, this mechanism was recently observed in Au nanowhiskers under compression along the [110] direction using a flat punch [13], a configuration which is characterized by a highly localized stress state under the tip, as in the classical nanoindentation case. Nevertheless, the plastic deformation processes change in the case of Wulff-shaped NPs compressed using a flat punch force field contacting the {001} or {111} facets (Figures 3E and 3F, respectively), where the joint nucleation of Shockley partial dislocations and nanotwins is observed. However, while NPs compressed along the <001> type directions show nanotwins with particularly large thicknesses (Figure 3E), only two-layer nanotwins are observed in <111>-oriented Wulff-shaped NPs (Figure 3F), similar to those observed in our *in situ* TEM nanocompression tests. These results were reproduced using two other interatomic potentials [47, 48] which cancels the hypothesis of a bias induced by the atomic interaction model.

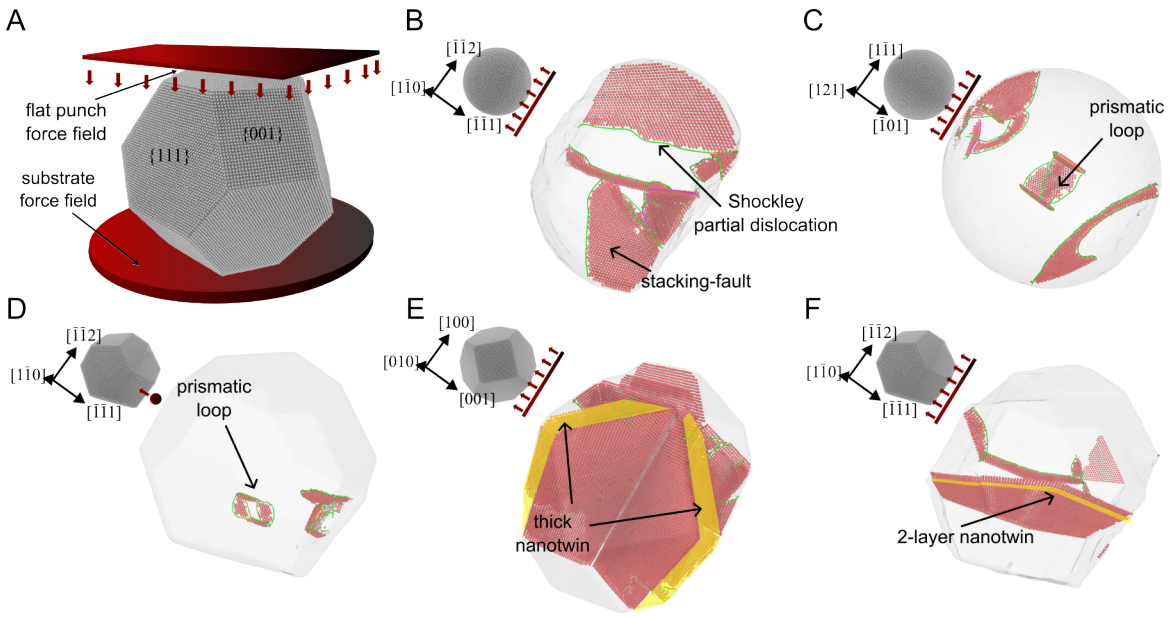

Fig. 3: MD simulation of Ag NPs under compression or indentation, A) MD compression protocol using force fields as substrate and indenter (flat punch illustrated as an example), B) nanocompression of <111> oriented Ag nanosphere (flat punch), C) nanocompression of <110> oriented Ag nanosphere (flat punch), D) nanoindentation of a <111> oriented Wulff-shaped Ag NP (spherical indenter), E) nanocompression of a <001> oriented Wulff-shaped Ag NP (flat punch), and F) nanocompression of a <111>-oriented Wulff-shaped Ag NP (flat punch). Surface atoms are colored in grey, stacking-faults and twin boundaries are characterized by local crystalline structure (HCP stacking) and colored in red, partial dislocations are colored in green, and nanotwin domains are highlighted in yellow. FCC perfect crystal atoms have been removed for the sake of clarity. The NPs and indenter shapes, as well as the direction of compression, are shown in the insets.

The various cases investigated in the simulation provide a clear picture of the deformation processes driving the plastic deformation of FCC Ag NPs. First, 1/6<112>{111} partial dislocations are observed in all the cases. They can either be uncorrelated leading to the formation of extended stacking-faults or correlated (as in the bulk material) leading to the slip system activation depends on the compression axis and stress concentration. Secondly, prismatic loops can be expelled from the surface in case of indentation using a shaped tip or compression of

spherical NPs. Those two cases are typical of highly concentrated and localized stress. Lastly, Ag NPs can deform by the nucleation and propagation of nanotwins but only for certain orientations. Sharma et al. [49] have recently discussed dislocation-based processes that operate during the compression of <111> oriented Ag hemispheres, emphasizing the lack of twins in the system, despite the low stacking-fault energy of Ag [50]. While the same conclusion applies here for <111>-oriented Ag nanospheres, nanotwins are observed for <111> and <001>-oriented Wulff-shaped NPs. While <001> oriented samples show particularly thick twins (more than three layers), which are relevant in the deformation process, their proportion is reduced (but not zero) in the case of <111>-faceted NPs where only a few two-layer nanotwins have been observed in both *in-situ* nanocompression experiments and MD simulations. The lack of twins in <111>-oriented FCC metals under compression can be justified using a classical Schmid approach, which suggests pure dislocation glide [51]. While two-layer nanotwins were lacking in the MD simulation of <111>-oriented hemispheres [49], their occurrence in <111>-oriented Wulff NPs is another confirmation of the influence of shape on the elementary deformation mechanisms of NPs [40, 52, 53].

Despite the experimental observation of nanotwins, we were unable to detect their nucleation in real-time, during the experiment (see movie clip in the supported file), due to their extreme velocity, which can reach a significant fraction of the speed of sound (3650 m/s in Ag) for shear stresses near the theoretical critical shear strength [54-56]. These velocities are associated with a time scale in the order of picoseconds (10^{-12} s) for the distance traveled along the NP. While such a time scale is typical of MD simulations, it is not yet possible to capture dislocations at such speeds in real time using CCD, CMOS, or even direct electron cameras, in conventional electron microscopes. Currently, the only option is to use dedicated time-resolved electron microscopes which can match the timescale of atomic-scale motions down to attoseconds [57,58,59]. So, the nanotwin was characterized immediately after stopping the deformation. Ultimately, the stability of dislocations within a NP is strongly dependent on the image stresses which increase as the particle size decreases [24, 60]. Thus, dislocations are unstable in individual and isolated NPs below a critical size, and consequently are spontaneously ejected toward the NP surfaces in the absence of applied stress.

To better assess the stability of the dislocations in Ag NPs, additional MD simulations were performed using the <111> oriented Wulff-shaped NP and the virtual flat punch. As shown in Figures 2E and 3F, a two-layer nanotwin like the one shown in the nanoindentation experiment, can be observed using this geometry. In particular, the aim was to investigate the relationship between the nanotwin dynamics and the image forces, by canceling the applied stress at various times during its propagation. For that purpose, four configurations corresponding to low (L), low-mid (LM), high-mid (HM), and high (H) positions of the nanotwin front in the NP were extracted from the master simulation and used as the starting points of a new simulation set, where the indenter is pushed backward at a constant rate. Figure 4 illustrates the respective configurations, before and after the withdrawal of the nanoindenter. The simulations show similar behavior for the L, LM, and HM cases (Figures 4A and 4B) where the nanotwin goes backward towards the surface, while for the H case, the nanotwin travels through the entire NP, reaching the opposite surface from where it had just nucleated after the indenter is removed (Figures 4C and 4D). These results were obtained by moving back the indenter at the same displacement rate as during the indentation without any steady-state stage. One may note that maintaining the indenter for too long at a fixed position, after the nucleation of the nanotwin, leads to the propagation of the twin (for all the L, LM, HM, and H cases) as it maintains an elevated applied stress in the range of the critical compressive stress for twin nucleation.

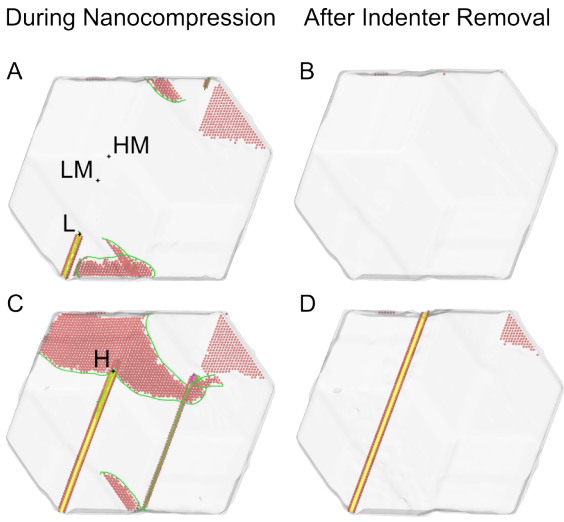

Fig. 4: MD simulations of the two-layer nanotwin stability as a function of its progression inside the Ag NP. Four positions of the twin front labeled as low (L), low-mid (LM), high-mid (HM), and high (H) in reference to the twin front position inside the NP are investigated. A) L, LM, and HM configurations under compressive stress. Only the L configuration is shown for the sake of clarity. Additional LM and HM positions are labeled using black crosses. B) L, LM, and HM configurations after removing the indenter (without applied stress). C) H configuration under compressive stress. D) H configuration after withdrawing the indenter. For all Figures, perfect crystal lattices are not shown but the NP surface is shown in transparent light grey. Stacking-faults and twin boundaries are characterized by atoms colored in red (HCP environment), partial dislocations are emphasized by green curves using the DXA algorithm, and nanotwin domains are highlighted in yellow.

These results can be rationalized using both image forces and energy balance arguments. On the one hand, while the nanotwin front is still near the nucleating surface (L, LM, and HM cases), it is energetically more favorable to travel back and eliminate the extrinsic planar fault and the surface steps generated by the defect propagation once the applied stress is removed. On the other hand, when the twin front is closer to the opposite surface, and the indenter is removed, the image forces induced by the opposite surface are strong enough to extend the nanotwin to cross the entire NP. This explains why nanotwinned domains are stable once they have entirely crossed the NP, even after the indenter is removed, in contrast to other dislocations that are ejected and will not leave any trace, nor will be observed due their speed and limitations of the camera. Thus, the front of the two-layer nanotwin observed in the experiments must still be near the surface to disappear once the indenter is removed. To determine the image stress τ acting on the dislocations during the *in-situ* experiment we consider the following expression [61]:

$$\tau = K \frac{G_1 b}{4\pi} \frac{2-\nu}{2(1-\nu)} \frac{1}{d} \quad (1)$$

where,

$$K = \frac{G_2 - G_1}{G_2 + G_1} \quad (2)$$

and G_1 = 24 GPa is the shear modulus for silver, G_2=0 is the shear modulus for vacuum, b is the Burgers vector of the partial dislocations, v = 0.37 is the Poisson ratio of silver, and d is the distance between a dislocation and the nearest NP surface. For the configuration shown in Figure 2B $b_{partial} = \frac{a}{6}\sqrt{(-2)^2 + (-1)^2 + (-1)^2}$= 1.66 Å and d is approximately 4 nm for the partial dislocation. This leads to an image stress of about 455 MPa for the partial dislocations associated with the nanotwin, which is above the average yield stress for polycrystalline silver that is 45 MPa. Note that such process should depend on the sample size. For the case of a silver single crystal the resolved shear stress is orientation dependent and related with the Schmid factor, which is much less than the yield stress for polycrystalline silver. This confirms that for such configurations, these defects should be ejected out by the surfaces.

Conclusions

In this study, we use aberration-corrected *in-situ* TEM to investigate the deformation of a 20 nm size Ag NP under compression along <111>. In particular, a two-layer nanotwin was identified before it left the sample upon removing the indenter. Using MD simulations, we have shown that the shape of both the Ag NPs and the indenter, as well as the orientation, play key roles in the type of defect that nucleates at the surface of the NP. While the <111> orientation generally impedes dislocation twinning in FCC metals, nanotwins are observed in our case due to a particularly heavy stress state induced by the faceted shape of the FCC Ag NP. The defect stability within the NP is also discussed. Both the simulations and the derived model confirm that within a critical distance traveled inside the NP, two-layer nanotwins can reverse and subsequently eject from the surface. On the other hand, if this critical distance is exceeded, the two-layer nanotwins will cross the entire sample because of the attractive image forces. Overall, it seems that the mechanisms of deformation acting on individual single-crystal metallic NPs below 20 nm are similar to those present in larger particles, i.e., by dislocation nucleation and glide. However, the smaller the NPs, the higher the tendency to experience the effect of nearby surfaces and the associated image stresses. Consequently, smaller NPs will be likely self-healing, thereby ejecting dislocations towards the free surfaces.

METHODS

In-situ Aberration-Corrected TEM Nanocompression

Nearly-spherical Ag NPs, provided by Novacentrix™, with a nominal size of 20 nm, were first affixed to a gold metal wire by dry dipping. In dry dipping, the wire is held by tweezers and dipped directly into a dry powder of NPs. During this process, the particles adhere to the wire due to Van der Waals forces. The wire supporting the Ag powder is then inserted into a Nanofactory instruments holder, which is located opposite to the probe. The nanoindenter tungsten probes for the specimen holder were purchased from Zyvex instruments. The tungsten probe was carefully affixed to the moving end of the specimen holder, which was then inserted into the TEM column. To conduct the *in-situ* nanocompression experiments, the W probe and the sample (silver NPs supported on a gold wire) were brought close to one another, and the image wobbler (automated variation of the objective lens current) was used to make sure the selected NP and the indenter were both in the focal plane. Under these conditions, the probe is expected to make contact if translated toward the NP. Subsequently, the Ag NPs were compressed *in-situ* by the W indenter, which due to its large radius of curvature, acts as a flat punch. The indenter was displaced perpendicularly to the $(1\overline{1}\overline{1})$ surface of the NP at a constant rate of 4 Å/s. The NP was imaged at 30 frames/second by a CCD camera, coupled to a double aberration-corrected JEOL 2200FS transmission electron microscope (TEM), operated at 200 kV and located at Brookhaven National Laboratory. We have used a defocus value of 14 Å and a spherical aberration coefficient of 1 μm, which was then used for computing the contrast transfer function. Phase contrast TEM images were acquired upon initial contact with the indenter and during each increment of displacement. One last snapshot was taken after the indenter removal. Force measurements were not taken during the experiments because the non-ideal shapes of the indenter and NP would make accurate estimates of the stress very difficult to determine, even if the forces were known.

Molecular Dynamics Simulations

MD simulations of Ag NPs under compression are performed using the open-source code LAMMPS [62]. Simulations are carried out using the embedded-atom method (EAM) and the interatomic potential of Zhou et al. [63, 64] commonly used to model Ag alloy properties including dislocation nucleation (see e.g. [49] and references therein). Additional simulations were also performed using the Adams and the Williams interatomic potentials for comparison [47,48]. Here

experimental NPs being particularly small with non-regular shapes, various shapes (with characteristic sizes of 20 to 25 nm), and orientations are investigated in the simulation including nanospheres and <110>- and <111>-oriented Wulff-shape NPs as designed using Atomsk [65] and the Wulff pack Python package [66]. Prior to compression, the potential energy of the system is first minimized at 0 K using a force norm criterion $f_{norm} \leq 10^{-6}$ eV/Å before equilibration consecutively in the NVE (30 ps) and NVT (50 ps) ensembles with a final temperature of 5 or 300 K monitored using the Nosé-Hoover thermostat. All MD simulations are performed using a timestep of 2 fs and free-boundary conditions. Nanocompression is modeled using the force-field method as already described in [32, 40]. Compression is performed by displacing the top (flat or spherical) force field towards the NP at a constant displacement rate equivalent to a longitudinal strain rate of $\dot{\varepsilon_{zz}}=10^8$ /s typical of MD simulations calculated along the vertical axis. In contrast, the bottom force field is kept fixed. A comparison between displacement- and load-control nanocompression simulations applied to FCC NPs is presented in [56]. Finally, atomic configurations are analyzed using the polyhedral template matching algorithm [67] and the dislocation extraction algorithm (DXA) [68] as implemented in Ovito [69].

Acknowledgements

The authors would like to thank Oleg Lourie from EDAX, for assisting with the *in-situ* nanocompression holder. The authors would like also to acknowledge the graphic work performed by Dr. Francisca Aroso from the University of Texas at Austin. Work at Brookhaven was supported by US DOE-BES, Materials Science and Engineering Division under Contract No: DE-SC0012704. The authors also acknowledge Fundação para a Ciência e a Tecnologia (FCT) for its financial support via the project LAETA Base Funding (DOI: 10.54499/UIDB/50022/2020), as well the Generalitat Valenciana through PROMETEO 2021/017 and the mobility grant PRX16/00519 of the Spanish Ministerio de Educación, Cultura y Deporte, and by the Agence Nationale de la Recherche, grant no. ANR-20-CE09-0015 (ANR SASHA). Centre de Calcul Intensif d'Aix-Marseille is acknowledged for granting access to its high-performance computing resources. The authors declare no competing financial interest.

References

[1] J.K. Patra, G. Das, L.F. Fraceto, E. Campos, M. Rodriguez-Torres, L. Acosta-Torres, L. Diaz-Torres, R. Grillo, M. Swamy, S. Sharma, S. Habtemariam, HS. Shin10, "Nano based drug delivery systems: recent developments and future prospects", Journal of Nanobiotechnology, 16:71, (2018)

[2] D. Guo, G. Xie and J. Luo, "Mechanical properties of nanoparticles: basics and applications", Journal of Physics D: Applied Physics, 47, 013001, (2014)

[3] T. Pingel, M. Jørgensen, A. Yankovich, H. Grönbeck, E. Olsson, " Influence of atomic site-specific strain on catalytic activity of supported nanoparticles", Nature Communications, 9, 2722, (2018)

[4] S.E. Temmel, E. Fabbri, D. Pergolesi, T. Lippert, T.J. Schmidt, "Investigating the role of strain toward the oxygen reduction activity on model thin film Pt catalysts", ACS Catalysis. 6, 7566–7576 (2016).

[5] A. van Bommel, and R. Divigalpitiya, "Effect of Calendering LiFePO4 Electrodes", Journal of The Electrochemical Society, 159, 11, A1791, (2012)

[6] J. Schiotz, K. Jacobsen, "A Maximum in the Strength of Nanocrystalline Copper", Science 301, 1357-1359, (2003).

[7] R.C. Hugo, H.H. Kung, J.R. Weertman, R. Mitra, J.A. Knapp, D.M. Follstaedt, "In situ TEM Tensile Testing of DC Magnetron Sputtered and Pulsed Laser Deposited Ni Thin Films", Acta Materialia 51, 1937-1943, (2003).

[8] A.M. Minor, S.A. Asif, Z. Shan, E.A. Stach, E. Cyrankowski, T.J. Wyrobek, O.L. Warren, "A new view of the onset of plasticity during the nanocompression of aluminium", Nature Materials 5, 697-702, (2006).

[9] E. Rabkin, D. Srolovitz, "Onset of plasticity in gold nanopillar compression", Nano Lett 7, 101-107, (2007).

[10] M.B. Lowry, D. Kiener, M.M. LeBlanc, C. Chisholm, J.N. Florando, J.W. Morris, A. Minor, "Achieving the ideal strength in annealed molybdenum nanopillars", Acta Materialia 58, 5160-5167, (2010).

[11] O. Kraft, P.A. Gruber, R. Mönig, Plasticity in confined dimensions, Annual Review of Materials Research. 40, 293–317, (2010)

[12] J. Greer, J.D. Hosson, Plasticity in small-sized metallic systems: intrinsic versus extrinsic size effect, Progress in Materials Science. 56, 654–724, (2011)

[13] S. Lee, A. Vaid, J. Im, B. Kim, A. Prakash, J. Guénolé, D. Kiener, E. Bitzek, S. H. Oh, "In situ observation of the initiation of plasticity by nucleation of prismatic dislocation loops", Nat. Communications 11, 1–11, (2020).

[14] J. Wang, Z. Zheng, C.R. Weinberger, Z. Zhang, T. Zhu, S.X Mao, "In situ atomic scale observation of twinning dominated deformation in nanoscale body-centred cubic tungsten", Nature Materials, 14, 594-600, (2015)

[15] M. Sorensen, M. Brandbyge, K. Jacobsen, "Mechanical deformation of atomic-scale metallic contacts: Structure and mechanisms", Physical Review B 57, 3283-3294, (1998)

[16] T. Kizuka, "Atomic process of point contact in gold studied by time-resolved high-resolution transmission electron microscopy", Physical Review Letters 81, 4448-4451, (1998).

[17] L. Sun, A. Krasheninnikov, T. Ahlgren, K. Nordlund, F. Banhart, "Plastic deformation of single nanometer-sized crystals", Physical Review Letters 101, 156-101, (2008)

[18] H. Zheng, A. Cao, C. Weinberger, J. Huang, K. Du, J. Wang, Y. Ma, Y. Xia, S. Mao, "Discrete plasticity in sub-10-nm-sized gold crystals", Nature Communications, 1, 144, (2008).

[19] L. Zhong, Y. Zhang, X. Wang, T. Zhu, S.X, Mao, "Atomic-scale observation of nucleation and growth-controlled deformation twinning in body-centered cubic nanocrystals", Nature Communications, 15:560, 1-9, (2024)

[20] D. Guo, G. Xie, J. Luo, Mechanical properties of nanoparticles: basics and applications, J. Phys. D: Appl. Phys. 47 013001, (2014)

[21] D. Mordehai, O. David, R. Kositski, Nucleation-controlled plasticity of metallic nanowires and nanoparticles, Advanced Materials. 305, 1706710–17, (2018)

[22] J. Amodeo, L. Pizzagalli, Modeling the mechanical properties of nanoparticles: a review, Comptes Rendus Physique. 22, 1–32, (2021)

[23] D. Maharaj, B. Bhushan, “Scale effects of nanomechanical properties and deformation behavior of Au NP and thin film using depth sensing nanocompression”, Beilstein J. Nanotechnol., 5, 822–836, (2014)

[24] Y. Wu, M. Takeguchi, Q. Chen, K. Furuya, “Defects and their movement in Pb and Ge nanocrystals characterized by ultra high vacuum high resolution transmission electron microscope”, Applied Surface Science 486, 159-160, (2000)

[25] W.W. Gerberich, W.M. Mook , C.R. Perrey , C.B. Carter ,M.I. Baskes , R. Mukherjee , A. Gidwani , J. Heberlein , P.H. McMurry , S.L. Girshick, “Superhard silicon nanospheres”, Journal of the Mechanics and Physics of Solids, 51, 979 – 992, (2003)

[26] W.W. Gerberich, W.M. Mook, M.J. Cordill, C.B. Carter, C.R. Perrey, J.V. Heberlein, S.L. Girshick, Reverse plasticity in single crystal silicon nanospheres, International Journal of Plasticity. 21, 2391–2405, (2005)

[27] D. Mordehai, M. Kazakevich, D. J. Srolovitz, E. Rabkin, “Nanocompression size effect in single-crystal NPs and thin films: A comparative experimental and simulation study”, Acta Materialia 59, 2309-2321, (2011)

[28] N. Zhang, Q.A. Deng, Y. Hong, L. Xiong, L. Shi, M. Strasberg, W. Yin, Y. Zou, C. R. Taylor, G. Sawyer, Y. Chen, “Deformation mechanisms in silicon NPs”, J. of Applied Physics 109, 063534, (2011)

[29] R. Kositski, D. Mordehai, “Depinning-controlled plastic deformation during nanocompression of BCC iron thin films and nanoparticles”, Acta Mater., 90, 370–379, (2015).

[30] C. E. Carlton, P. J. Ferreira, “In situ TEM Nanocompression of NPs”, Micron Special Issue 43, 1134-1139, (2012).

[31] J. Sun, L. He, YC. Lo, T. Xu, H. Bi, L. Sun, Z. Zhang, S.X. Mao, J. Li, “Liquid-like pseudoelasticity of sub-10-nm crystalline silver particles”, Nature Materials, 13, 1007-1012, (2014)

[32] I. Issa, J. Amodeo, J. Réthoré, L. Joly-Pottuz, C. Esnouf, J. Morthomas, M. Perez, J. Chevalier, K. Masenelli-Varlot, In situ investigation of MgO nanocube deformation at room temperature, Acta Materialia. 86, 295–304, (2015)

[33] I. Issa, L. Joly-Pottuz, J. Amodeo, D. J. Dunstan, C. Esnouf, J. Réthoré, V. Garnier, J. Chevalier & K. Masenelli-Varlot, From dislocation nucleation to dislocation multiplication in ceramic nanoparticle, Materials Research Letters, 9:6, 278-283, (2021)

[34] A.J. Wagner, E.D. Hintsala, P. Kumar, W.W. Gerberich, K.A. Mkhoyan, Mechanisms of plasticity in near-theoretical strength sub-100nm Si nanocubes, Acta Materialia. 100, 256–265, (2015)

[35] A. Parakh, S. Lee, K.A. Harkins, M.T. Kiani, D. Doan, M. Kunz, A. Doran, L.A. Hanson, S. Ryu, X.W. Gu, "Nucleation of dislocations in 3.9 nm nanocrystals at high pressure", Physical Review Letters, 124, 106104, (2020)

[36] A. Parakh, S. Lee, M.T Kiani, D Loan, M. Kunz, A. Doran, S. Ryu, X.W. Gu, "Stress-induced structural transformations in Au nanocrystals", Nano Letters, 20, 7767-7773, (2020)

[37] S. Chen, F. Liu, B. Liu, X. Chen, X. Ke, M. Zhang, X. Tang, P. Guan, Z. Zhang, Z. Shan, Q. Yu, Reaching near-theoretical strength by achieving quasi-homogenous surface dislocation nucleation in MgO particles, Mater Today. 37–45, (2022)

[38] Gómez-Rodríguez, A., Beltrán-del-Río, L. M., & Herrera-Becerra, R. SimulaTEM: Multislice simulations for general objects. Ultramicroscopy, 110(2), 95–104, (2010)

[39] J.D. Nowak, A.R. Beaber, O. Ugurlu, S.L. Girshick, W.W. Gerberich, Small size strength dependence on dislocation nucleation, Scripta Materialia. 62, 819–822, (2010)

[40] J. Amodeo, K. Lizoul, Mechanical properties and dislocation nucleation in nanocrystals with blunt edges, Materials and Design. 135 223–231, (2017)

[41] S. Oh, M. Legros, D. Kiener, P. Gruber, G. Dehm, In situ TEM straining of single crystal Au films on polyimide : Change of deformation mechanisms at the nanoscale, Acta Materialia. 55, 5558–5571, (2007)

[42] C. E. Carlton, L. Rabenberg, P. J. Ferreira, "On the Nucleation of Partial Dislocations in nanoparticles", Philosophical Magazine Letters 88, 715-724, (2008).

[43] B. Roos, B. Kapelle, G. Richter, C.A. Volkert, Surface dislocation nucleation controlled deformation of Au nanowires, Applied Physics Letters. 105, 201908, (2014)

[44] S. Yoshida, M. Kiritani and Y. Shimomura, Dislocation loops with stacking fault in quenched aluminum. *Journal of the Physical Society of Japan*, *18*(2), 175-183, (1963)

[45] V. Gavini, K. Bhattacharya and M. Ortiz, Vacancy clustering and prismatic dislocation loop formation in aluminum. *Physical Review B*, *76* (18), 18010, (2007)

[46] H.-J. Chang, M. Fivel, D. Rodney, M. Verdier, Multiscale modelling of indentation in FCC metals: From atomic to continuum, Comptes Rendus Physique. 11, 285–292, (2010)

[47] J.B. Adams, S.M. Foiles, W.G. Wolfer, Self-diffusion and impurity diffusion of fee metals using the five-frequency model and the Embedded Atom Method, Journal of Materials Research. 4, 102–112, (1989)

[48] P.L. Williams, Y. Mishin, J.C. Hamilton, An embedded-atom potential for the Cu–Ag system, Model Simul Mater Sc. 14, 817, (2006)

[49] A. Sharma, J. Amodeo, N. Gazit, Y. Qi, O. Thomas, E. Rabkin, When More Is Less: Plastic Weakening of Single Crystalline Ag Nanoparticles by the Polycrystalline Au Shell, Acs Nano. 9, 14061–14070, (2021)

[50] E.B. Tadmor, N. Bernstein, A first-principles measure for the twinnability of FCC metals, J Mech Phys Solids. 52, 2507–2519, (2004)

[51] S. Xu, Y.F. Guo, A.H.W. Ngan, A molecular dynamics study on the orientation, size, and dislocation confinement effects on the plastic deformation of Al nanopillars, Int J Plasticity. 43, 116–127, (2013)

[52] D. Kilymis, C. Gerard, J. Amodeo, U.V. Waghmare, L. Pizzagalli, Uniaxial compression of silicon nanoparticles: An atomistic study on the shape and size effects, Acta Materialia. 158, 155–166, (2018)

[53] A. Sharma, J. Hickman, N. Gazit, E. Rabkin, Y. Mishin, Nickel nanoparticles set a new record of strength, Nature Communications. 9, 1–9, (2018)

[54] P. Gumbsch, H. Gao, Driving force and nucleation of supersonic dislocations, J Comput-Aided Mater. 6, 137–144, (1999)

[55] J. Marian, A. Caro, Moving dislocations in disordered alloys: Connecting continuum and discrete models with atomistic simulations, Phys Rev B. 74, (2006)

[56] H. Iteney, T.W. Cornelius, O. Thomas, J. Amodeo, Load versus displacement-controlled nanocompression: Insights from atomistic simulations, Scripta Mater. 226, 115245, (2023)

[57] K. E. Priebe, C. Rathje, S. V. Yalunin, T. Hohage, A. Feist, S. Sch€afer, and C. Ropers, Nat. Photonics 11, 793 (2017).

[58] Y. Morimoto and P. Baum, Nat. Phys. 14, 252 (2018).

[59] N. Sch€onenberger, A. Mittelbach, P. Yousefi, J. McNeur, U. Niedermayer, and P. Hommelhoff, Phys. Rev. Lett. 123, 264803 (2019).

[60] L. Sun, A. Krasheninnikov, T. Ahlgren, K. Nordlund, F. Banhart, "Plastic deformation of single nanometer-sized crystals", Physical Review Letters 101, 156-101, (2008).

[61] Y. Estrin, V. Lemiale, R. O'donnell, L. Toth, "On Homogeneous Nucleation of Dislocation Loops in Nanocrystalline Materials", Metallurgical and Materials Transactions A 42, 3883-3888, (2011).

[62] A.P. Thompson, H.M. Aktulga, R. Berger, D.S. Bolintineanu, W.M. Brown, P.S. Crozier, P.J. in 't Veld, A. Kohlmeyer, S.G. Moore, T.D. Nguyen, R. Shan, M.J. Stevens, J. Tranchida, C. Trott, S.J. Plimpton, "LAMMPS - a flexible simulation tool for particle-based materials modeling at the atomic, meso, and continuum scales", Comput Phys Commun. 271 108171, (2022).

[63] X.W. Zhou, H.N.G. Wadley, R.A. Johnson, D.J. Larson, N. Tabat, A. Cerezo, A.K. Petford-Long, G.D.W. Smith, P.H. Clifton, R.L. Martens, T.F. Kelly, Atomic scale structure of sputtered metal multilayers, Acta Materialia. 49, 4005–4015, (2001)

[64] X.W. Zhou, R.A. Johnson, H.N.G. Wadley, Misfit-energy-increasing dislocations in vapor-deposited CoFe/NiFe multilayers, Physical Review B. 69, 1358–10, (2004)

[65] P. Hirel, Atomsk: A tool for manipulating and converting atomic data files, Computer Physics Communications. 197, 212–219, (2015)

[66] J. Rahm, P. Erhart, WulffPack: A Python package for Wulff constructions, J Open Source Softw. 5, 1944, (2020)

[67] P.M. Larsen, S. Schmidt, J. Schiøtz, Robust structural identification via polyhedral template matching, Modelling and Simulation in Materials Science and Engineering. 24, 055007–19, (2016)

[68] A. Stukowski, Computational Analysis Methods in Atomistic Modeling of Crystals, JOM. 66, 399–407, (2014)

[69] A. Stukowski, Visualization and analysis of atomistic simulation data with OVITO-the Open Visualization Tool, Modelling and Simulation in Materials Science and Engineering. 18, 7pp., (2010)